

Teilprojekt B2.15

Topologically-Protected Low Dimensional Metals

Principal Investigator: Alexander Mirlin

CFN financed scientists: Dmitry Gutman, Christian Seiler

Further contributing scientists: Dmitry Bagrets, Ferdinand Evers, Ivan Protopopov, Igor Gornyi, Elio König, Pavel Ostrovsky, Martin Schneider

**Institut für Theorie der Kondensierten Materie
KIT Campus Süd**

**Institut für Nanotechnologie
KIT Campus Nord**

Introduction

The Project deals with topologically protected metals and insulators in low-dimensional structures. Such systems are typically characterized by a linear Dirac-type dispersion of the conducting modes. Solid state systems with massless Dirac charge carriers have recently attracted an outstanding attention of leading theoretical and experimental groups. This is mainly due to the impressive experimental progress in the two technically different but conceptually similar directions of research: graphene and topological insulators. The notion of topological insulator refers to a bulk band insulator with gapless surface states occurring due to topological reasons. The simplest example of a topological insulator is the 2D electron gas in a strong magnetic field. At the quantum Hall plateau, the gap between Landau levels in the bulk is penetrated by a fixed integer number of chiral edge states providing the quantized value of the Hall conductance.

A similar effect was recently discovered in systems without magnetic field (time-reversal symmetry is preserved) but with strong spin-orbit interaction. The existence of a non-localized conducting channel at the edge of a 2D HgTe/CdHgTe quantum well was experimentally demonstrated [1]. Strong spin-orbit interaction in HgTe leads to the inverted band gap in this semiconductor. As a result, the electron and hole bands are crossing near the boundary of the sample giving rise to the two counter-propagating spin-polarized edge modes. The time-reversal symmetry of the system leads to the topological protection of these edge modes. Voltage applied to such a sample results in the appearance of the perpendicular spin current. This phenomenon is known as the quantum spin-Hall effect (QSHE). The robustness of the effect with respect to disorder makes it an extremely promising tool for applications. As a simplest example, the conversion between the usual charge current and spin current occurring in QSHE can be used for generation and detection of spin currents.

The 3D analogue of QSHE was very recently realized in the Bi-based alloys [2]. The 3D topological insulators exhibit very strong spin-orbit interaction also leading to the band gap inversion. This results in the appearance of gapless states on the surface of the sample. The dynamics of the surface states is governed by the same massless Dirac Hamiltonian that has previously appeared in graphene. The main difference between graphene and the surface of a 3D topological insulator is the lack of the spin and valley degeneracy in the latter case. The absence of an additional degeneracy of the spectrum results in the lack of screening and hence in considerably stronger interaction effects in topological insulators as compared to graphene.

Besides exciting physical properties, the topological protection renders such systems promising candidates for a variety of prospective electronic and spintronic devices. It is thus of crucial importance to understand properties of boundary metallic modes in the realistic systems when both disorder and interaction are present.

In this project, we study topological-insulator phases, with the focus on *topologically protected low-dimensional metals* on their boundaries. The objectives of the project include:

I. Topological insulators and superconductors

This part of the Project is devoted to phenomena arising in both 2D and 3D topological insulators due to various types of disorder, interaction, magnetic field, optical irradiation and their interplay. In all the problems, particular attention will be paid to the effects of Coulomb interaction. The results obtained within the Project concern the combined effect of disorder and interaction on the transport properties of both 2D and 3D samples [B2.15:3]. We have predicted the novel interaction-

induced critical state on the surface of 3D topological insulators with the conductivity of order e^2/h . This critical state appears automatically, without any fine tuning of parameters, and hence can be called *self-organized quantum criticality*. This critical state is now searched for by the Princeton University experimental group (Checkelsky, Ong, Hasan). In the 2D case, the Coulomb interaction results in the direct transition (quantum spin-Hall transition) between the two distinct insulating phases (ordinary and topological insulator) via another novel quantum-spin-Hall critical state. The quantum spin-Hall transition and signatures of critical behaviour were recently observed in HgTe quantum wells [3].

More specifically, in this part of the Project we study:

I.1. *Interaction and disorder effects in topological insulators.*

I.2. *Quantum spin-Hall effect.*

I.3. *Optics of topological insulators.*

I.4. *Topological insulators in external magnetic field.*

I.5. *Superconductor-topological insulator junctions.*

II. Dephasing and nonequilibrium phenomena in topologically protected metals

II.1. *Dephasing at criticality*

II.2. *Nonequilibrium effects and dephasing in edge state interferometers*

Finally, we explore possibilities of *applications* of such topologically protected systems as devices for *spintronics* and *quantum computing*. The work in this project is carried out in cooperation with several CFN projects, including theoretical and experimental activities in the field of quantum computing and superconducting nanostructures (in particular, topologically protected qubits; Ustinov, von Löhneysen, Schön, Shnirman) as well as spintronics (Shnirman, Schön).

1. Symmetry classification of topological insulators and superconductors

Critical phenomena and quantum phase transitions are paradigmatic concepts in modern condensed matter physics. The universality of critical phenomena has been studied both in the area of strongly correlated systems and in mesoscopics. A central example in the field of mesoscopic physics is the localization-delocalization (metal-insulator) quantum phase transition driven by disorder --- the Anderson transition [4]. Although the notion of localization has appeared half a century ago, this field is still full of surprising new developments. One of the most recent arenas where novel peculiar localization phenomena have been studied is physics of topological insulators, i.e., bulk insulators with delocalized (topologically protected) states on their surface. In Refs. [B2.15:1, B2.15:2, B2.15:3] we have addressed the symmetry-based classification of topological insulators and superconductors.

It is now established that disordered electronic systems can be classified into 10 symmetry classes (for review see Refs. [4, B2.15:1, B2.15:2]). The localization properties are determined by the symmetry class and dimensionality of the system. The critical behavior of a system depends also on the underlying topology. This is particularly relevant for topological insulators. The famous example of a topological insulator (TI) is a two-dimensional (2D) system on one of quantum Hall (QH) plateaus in the integer quantum Hall effect (QHE). Such a system is characterized by an integer (Chern number) $n = \dots, -2, -1, 0, 1, 2, \dots$ which counts the edge states (the sign determines direction of chiral edge modes). The integer QH edge is thus a topologically protected one-dimensional (1D) conductor realizing the group \mathbb{Z} . Another (\mathbb{Z}_2) class of topological insulators can be realized in systems with strong spin-orbit interaction and without magnetic field (class AII) --- and was discovered in 2D HgTe/HgCdTe structures in Ref. [1]. A 3D \mathbb{Z}_2 topological insulator [2] has been found and investigated for the first time in $\text{Bi}_{1-x}\text{Sb}_x$ crystals. Both in 2D and 3D, \mathbb{Z}_2

topological insulators are band insulators with the following properties: (i) time reversal invariance is preserved (unlike ordinary quantum Hall systems); (ii) there exists a topological invariant, which is similar to the Chern number in QHE; (iii) this invariant belongs to the group Z_2 and reflects the presence or absence of delocalized edge modes (Kramers pairs).

Topological insulators exist in all ten symmetry classes in different dimensions, see Table I. Very generally, the classification of topological insulators in d dimensions can be constructed by studying the Anderson localization problem in a $(d-1)$ -dimensional disordered system. Indeed, absence of localization of surface states due to the topological protection implies the topological character of the insulator. The full classification (periodic table) of topological insulators and superconductors for all ten symmetry classes was developed in Refs. [5] and [6]. This classification determines whether the Z or Z_2 topological insulator is possible in the d -dimensional system of a given symmetry class. In Refs. [B2.15:1, B2.15:2, B2.15:3] we discuss the connection between the classification schemes of these papers.

p	Symmetry classes			$\pi_0(R_p)$	Topological insulators			
	H_p	R_p	S_p		d=1	d=2	d=3	d=4
0	AI	BDI	CII	Z	0	0	0	Z
1	BDI	BD	AII	Z_2	Z	0	0	0
2	BD	DIII	DIII	Z_2	Z_2	Z	0	0
3	DIII	AII	BD	0	Z_2	Z_2	Z	0
4	AII	CII	BDI	Z	0	Z_2	Z_2	Z
5	CII	C	AI	0	Z	0	Z_2	Z_2
6	C	CI	CI	0	0	Z	0	Z_2
7	CI	AI	C	0	0	0	Z	0
0'	A	AIII	AIII	Z	0	Z	0	Z
1'	AIII	A	A	0	Z	0	Z	0

Table I. Symmetry classes and "Periodic Table" of topological insulators [5,6, B2.15:1, B2.15:2, B2.15:3]. The first column enumerates the symmetry classes of disordered systems which are defined as the symmetry classes H_p of the Hamiltonians (second column). The third column lists the symmetry classes of the classifying spaces (spaces of reduced Hamiltonians) [5]. The fourth column represents the symmetry classes of a compact sector of the sigma-model manifold. The fifth column displays the zeroth homotopy group $\pi_0(R_p)$ of the classifying space. The last four columns show the possibility of existence of Z and Z_2 topological insulators in each symmetry class in dimensions $d=1,2,3,4$.

All symmetry classes of disordered systems can be divided into two groups: $\{A, AIII\}$ and $\{\text{all other}\}$. The classes of the big group are labeled by $p=0,1,\dots,7$. Each class is characterized by (i) Hamiltonian symmetry class H_p ; (ii) symmetry class R_p of the classifying space used by Kitaev [5]; (iii) symmetry class S_p of the compact sector M_F of the sigma-model manifold. The symmetry class R_p of the classifying space of reduced Hamiltonians characterizes the space of matrices obtained from the Hamiltonian by keeping all eigenvectors and replacing all positive eigenvalues by +1 and all negative by -1. Note that

$$R_p = H_{p+1}, \quad S_p = R_{4-p}.$$

Here and below cyclic definition of indices $\{0,1,\dots,7\} \pmod{8}$ and $\{0',1'\} \pmod{2}$ is assumed.

For the classification of topological insulators it is important to know homotopy groups π_d for all symmetry classes. In Table I we list $\pi_0(R_p)$; other π_d are given by

$$\pi_d(R_p) = \pi_0(R_{p+d}).$$

The homotopy groups π_d have periodicity 8 (Bott periodicity).

There are two ways to detect topological insulators: by inspecting the topology of (i) classifying space R_p or of (ii) the sigma-model space S_p .

(i) Existence of topological insulator (TI) of class p in d dimensions is established by the homotopy group π_0 for the classifying space R_{p-d} :

$$\begin{cases} \text{TI of the type Z} \\ \text{TI of the type } Z_2 \end{cases} \iff \pi_0(R_{p-d}) = \begin{cases} Z \\ Z_2 \end{cases} \quad \pi_0(R_p) = \begin{cases} Z & \text{for } p = 0, 4, \\ Z_2 & \text{for } p = 1, 2. \end{cases}$$

(ii) Alternatively, the existence of topological insulator of symmetry class p in d dimensions can be inferred from the homotopy groups of the sigma-model manifolds, as follows:

$$\begin{cases} \text{TI of the type Z} \\ \text{TI of the type } Z_2 \end{cases} \iff \begin{cases} \pi_d(S_p) = Z \\ \pi_{d-1}(S_p) = Z_2 \end{cases}$$

The criterion (ii) is obtained if one requires existence of "non-localizable" boundary excitations. This may be guaranteed by either Wess-Zumino term in $d-1$ dimensions [which is equivalent to the Z topological term in d dimensions, i.e. $\pi_d(S_p) = Z$] for a QHE-type topological insulator, or by the Z_2 topological term in $d-1$ dimensions [i.e. $\pi_{d-1}(S_p) = Z_2$] for a QSH-type topological insulator. The above criteria (i) and (ii) are equivalent, since

$$\pi_d(S_p) = \pi_d(R_{4-p}) = \pi_0(R_{4-p+d}).$$

While the criterion (i) was proposed in Refs. [5,6], the criterion (ii) was established in Refs. [B2.15:1, B2.15:2, B2.15:3].

2. Topological protection of 2D metallic surface states

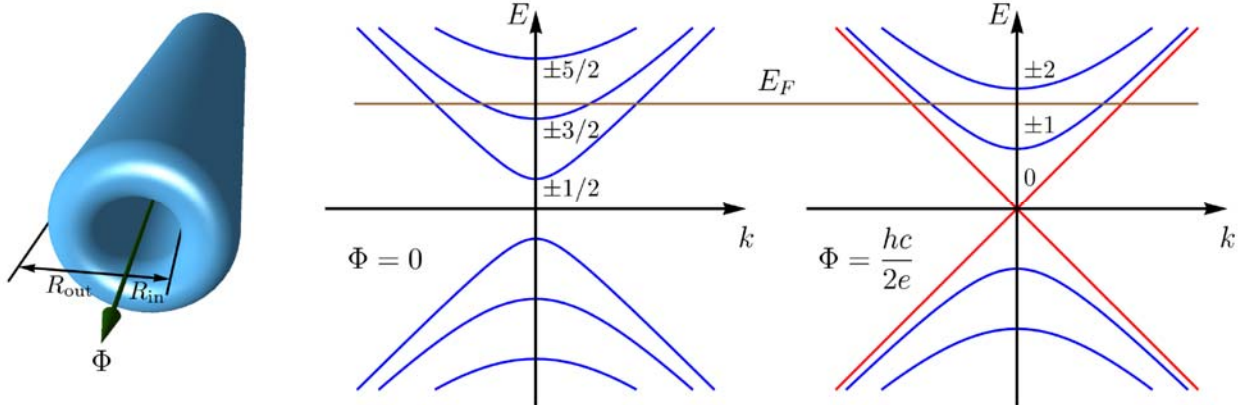


Fig. 1. *Left panel:* schematic illustration of the hollow cylinder sample used for proving the absence of localization on the surface of a 3D topological insulator. *Right panel:* the energy spectra of a clean

2D system on the surface of the cylinder with zero flux and with half of the magnetic flux quantum penetrating the cylinder.

In Ref. [B2.15:3] we have derived the effective surface Hamiltonian

$$H_{\text{surf}} = \frac{i}{2} [\sigma \mathbf{p}, \sigma \mathbf{n}] = \frac{\nabla \mathbf{n}}{2} + \frac{1}{2} (\mathbf{n}[\mathbf{p} \times \sigma] + [\mathbf{p} \times \sigma] \mathbf{n})$$

for 2D metallic states on the surface of a 3D Z_2 topological insulator (\mathbf{n} is the normal to the surface). Using this Hamiltonian, we have proved the topological protection of the surface states in the presence of disorder. Furthermore, we have discussed the stability of topological insulators with respect to electron-electron interaction. We have demonstrated that not too strong interactions do not affect the existence of the topological-insulator phase.

The proof for the non-interacting case can be outlined as follows. Consider the 2D system formed at the surface of a 3D topological insulator and described by the above Hamiltonian. Assume that all the states in 2D are localized with some localization length. Consider a hollow cylinder with all dimensions much larger than the localization length pierced by the Aharonov-Bohm magnetic flux $\Phi = hc/2e$ (half of the flux quantum), Fig. 1. This value of Φ does not break the time-reversal symmetry leaving the system in the symplectic class. In the absence of disorder we can characterize the surface states by the momentum k along the cylinder axis and by the integer angular momentum n . The energy of such a state is given by

$$E = \sqrt{k^2 + (n/R)^2}.$$

The channels with positive and negative n are degenerate, while $n = 0$ channel is not. Thus the cylinder sustains an odd number of conducting channels both on the inner and outer surface at any value of chemical potential. Now we include disorder and show the absence of localization in quasi-one-dimensional (q1D) symplectic system with odd number of channels. The scattering matrix of such a q1D wire has the form

$$S = \begin{pmatrix} r & t' \\ t & r' \end{pmatrix}$$

with transmission and reflection amplitudes as its entries. The blocks r and r' are square matrices of the size determined by the number of channels. Time-reversal symmetry of the symplectic type imposes the following restrictions on the amplitudes entering the matrix S :

$$r = -r^T, \quad r' = -r'^T, \quad t = t'^T.$$

Calculating the determinant of the both sides of the first identity and taking into account the odd size of the matrix r , we obtain $\det r = 0$. This implies a zero eigenvalue of r and hence the existence of a channel with perfect transmission. We conclude: in a q1D wire of symplectic symmetry with an odd number of channels one channel always remains delocalized. Applying the q1D result to the cylinder constructed above we immediately come to the controversy: in spite of assumed 2D localization on the surface, the infinitely long cylinder possesses two (inner and outer) conducting channels. This proves the absence of localization in 2D states on the surface of a 3D topological insulator.

The proof has been generalized to include the Coulomb interaction. We assume the temperature to be much smaller than the inverse time of electron propagation through the system. At such low temperatures the inelastic scattering of electrons is negligible and we can describe the transport by the *single-particle* scattering matrix calculated at the Fermi energy and accounting for virtual

processes. The latter renormalize the parameters of the S matrix, the renormalization being cut off by the system size. Assuming no interaction-induced breaking of the time-reversal symmetry, the symmetry properties of this S matrix are unchanged and hence the above proof applies. We have shown that this assumption is valid provided that the interaction (characterized by the dimensionless parameter $r_s \sim e^2/hv_F$) is not too strong. The persistence of topological protection of 2D surface states in the presence of interaction is encoded in the structure of the replicated Matsubara sigma-model. Similarly to the ordinary QHE, this theory possesses the same nontrivial topology as in the non-interacting case.

3. Interaction-induced criticality in topological insulators

In Ref. [B2.15:3] we have predicted a novel critical state which emerges due to the interplay of nontrivial topology and the Coulomb interaction.

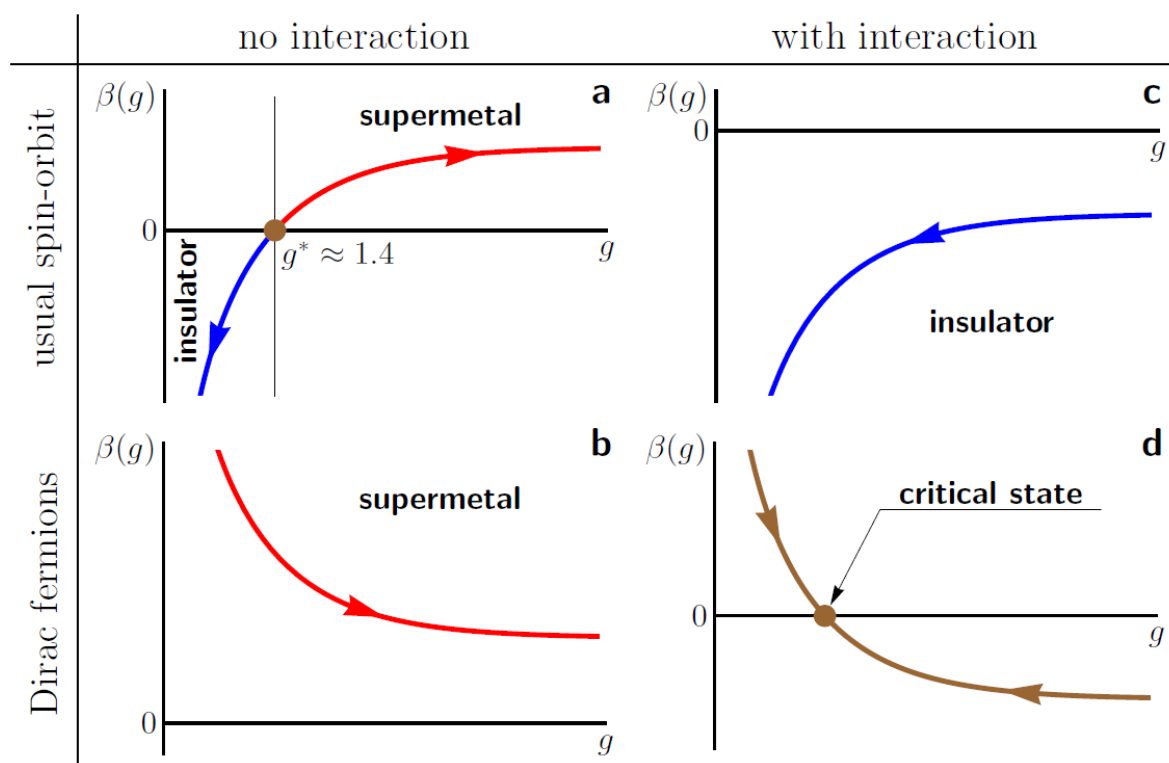


Fig. 2. Schematic scaling functions for the conductivity of 2D disordered systems of symplectic symmetry class. The plotted beta functions determine the flow of the dimensionless conductivity g with increasing system size L (as indicated by the arrows). The upper two panels show the beta functions for ordinary SO systems which are not topologically protected; the lower two panels demonstrate the scaling for topologically protected Dirac fermions (left: no interaction; right: Coulomb interaction included). In the interacting case the number of independent flavors is $N=1$.

Let us start with reviewing the localization properties of 2D systems of symplectic symmetry class AII without Coulomb interaction. In conventional SO systems (e.g. semiconductors with SO scattering), there are two phases: metal and insulator with the Anderson transition between them,

Fig. 2a. A qualitatively different situation occurs in a single species of massless Dirac fermions in a random scalar potential. This system also belongs to the symplectic symmetry class but its metallic phase is "topologically protected" whatever disorder strength. In terms of scaling, this means a positive beta function, $\beta(g)=dg/d\ln L>0$, for small dimensionless (in units e^2/h) conductivity g (see Fig. 2b). This topologically protected state has been recently predicted for disordered graphene with no spin- and no valley-mixing [7]. The absence of localization in this model has been confirmed in numerical simulations [8]. The scaling function has been found in Ref. [8] to be strictly positive, implying a flow towards the "supermetal" fixed point (see Fig. 2b). While a genuine single Dirac fermion cannot be realized in a truly 2D microscopic theory because of the "fermion doubling" problem, it emerges on the surface of a 3D TI.

Can the topologically protected 2D state be a supermetal as in the non-interacting case? To answer this question, we employed in Ref. [B2.15:3] the perturbative RG which is applicable for large conductivity $g \gg 1$. It is well known that in a 2D diffusive system the interaction leads to logarithmic corrections to the conductivity [9]. These corrections (together with the interference-induced ones) can be summed up with the use of RG technique [10]. The one-loop equation for renormalization of the conductivity in the symplectic class with long-range Coulomb interaction and a single species of particles has the following form:

$$\beta(g) = \frac{dg}{d\ln L} = -1/2.$$

Here $-1/2$ on the r.h.s. is a sum of the weak antilocalization correction $1/2$ due to disorder and -1 induced by the Coulomb interaction in the singlet channel. The negative interaction-induced term in the beta function dominates the scaling at large g . Therefore, for $g \gg 1$ the conductance decreases upon renormalization and the supermetal fixed point becomes repulsive.

Thus, on one hand, at $g \gg 1$ there is (i) scaling towards smaller g on the side of large g . On the other hand, surface states are topologically protected from localization, which yields (ii) scaling towards higher g on the side of small g . The combination of (i) and (ii) leads unavoidably to the conclusion that the system should scale to a critical state ($g \sim 1$). Indeed, there is no other way to continuously interpolate between negative (i) and positive (ii) beta functions: at some point beta function should cross zero. As a result, a critical point emerges due to the combined effect of interaction and topology. In other words, if the system can flow neither towards a supermetal nor to an insulator it must flow to an intermediate fixed point ($g \sim 1$). Remarkably, the critical state emerges on the surface of a 3D topological insulator without any adjustable parameters. This phenomenon can be thus called "self-organized quantum criticality".

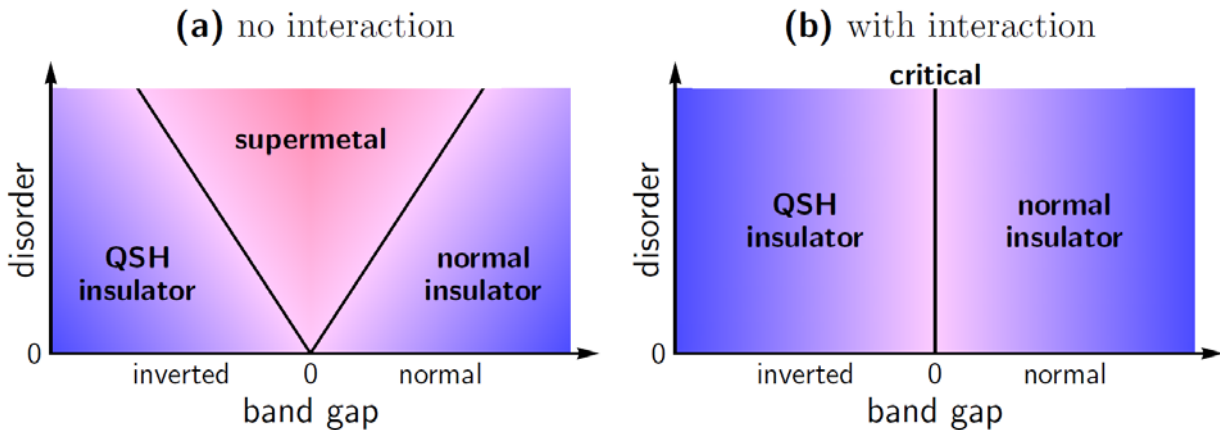


Fig. 3. The phase diagrams of a disordered 2D system demonstrating the QSH effect. *Left panel:* non-interacting case. *Right panel:* interacting case (with Coulomb interaction not screened by external gates). Interaction “kills” the supermetallic phase. Thus, the two insulating phases are separated by the critical line.

Let us now return to 2D QSH topological insulators. The 2D disordered QSH system contains only a single flavor of particles, $N = 1$. Indeed, the spin-orbit interaction breaks the spin-rotational symmetry, whereas the valleys are mixed by disorder. As a result, the supermetal phase does not survive in the presence of Coulomb interaction: at $g \gg 1$ the interaction-induced localization wins. This is analogous to the case of the surface of a 3D topological insulator discussed above.

The edge of a 2D topological insulator is protected from the full localization. This means that the topological distinction between the two insulating phases (ordinary and QSH insulator) is not destroyed by the interaction, whereas the supermetallic phase separating them disappears. Therefore, the transition between two insulators occurs through an interaction-induced critical state, see Fig. 3 (right panel).

Our predictions of quantum criticality resulting from interplay of disorder, interaction, and topological protection, can be verified via transport experiments. Such experiments are currently performed in Würzburg (transition from 2D topological insulator to normal insulator) and Princeton (surfaces of 3D topological insulators), and the preliminary results are in agreement with our predictions.

4. Dephasing at criticality

In Ref. [11] we have analyzed the critical behavior of the dephasing rate induced by short-range electron-electron interaction near an Anderson transition of metal-insulator or quantum Hall type. The corresponding exponent characterizes the scaling of the transition width with temperature. Assuming no spin degeneracy, the critical behavior has been studied by performing the scaling analysis in the vicinity of the non-interacting fixed point, since the latter is stable with respect to the interaction in this universality class.

We have combined an analytical treatment (that includes the identification of operators responsible for dephasing in the formalism of the non-linear sigma-model and the corresponding renormalization-group analysis in $2+\epsilon$ dimensions) with numerical simulations on the Chalker-Coddington network model of the quantum Hall transition. This allowed us to find the analytical results for the exponents governing the temperature scaling of the dephasing rate, dephasing length, and the transition width. Our numerical results for the exponents largely agree with those obtained in Refs. [12,13] (see Figs. 4 and 5). However, our system sizes are much larger than those studied in Ref. [13] that was crucial for getting a window of distances where corrections to power-law scaling are small.

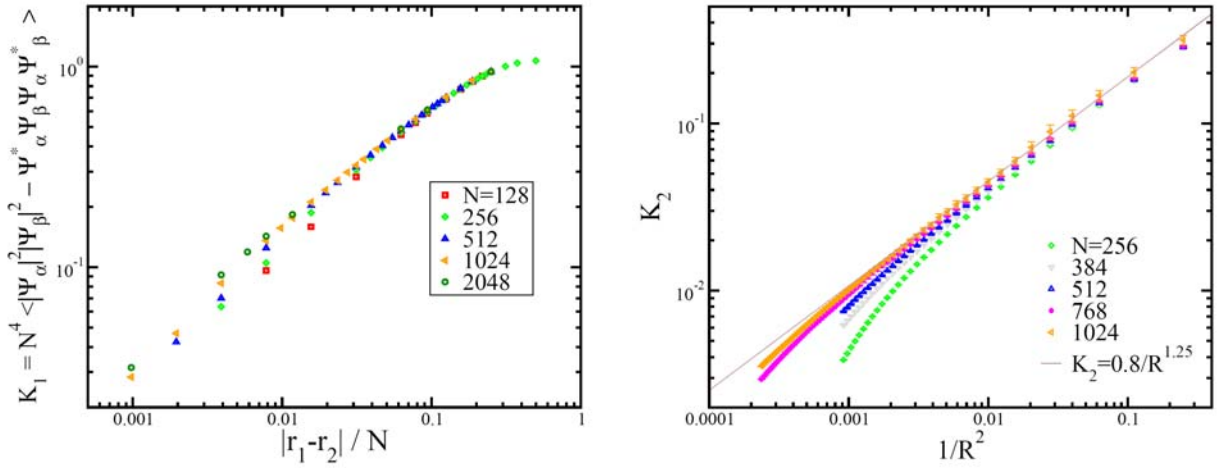


Fig. 4. *Left panel:* Scaling of product of four wave functions taken at two spatial positions K_1 (relevant for the Hartree-Fock matrix element) with the distance between the two points in the vicinity of the quantum-Hall transition. The leading power laws cancel and the effective strength of the interaction is determined by the subleading contributions. The extracted value of the power-law exponent is $\mu_2=0.625$ within the numerical uncertainty. *Right panel:* Scaling of the product of eight wave functions K_2 (which is relevant for the dephasing rate) with the distance R between the two couples of spatial points for different system sizes N . With increasing N , the data approach the straight line, corresponding to a power-law dependence. The corresponding exponent is ~ 1.25 , i.e. equal to $2\mu_2$ within the numerical uncertainty.

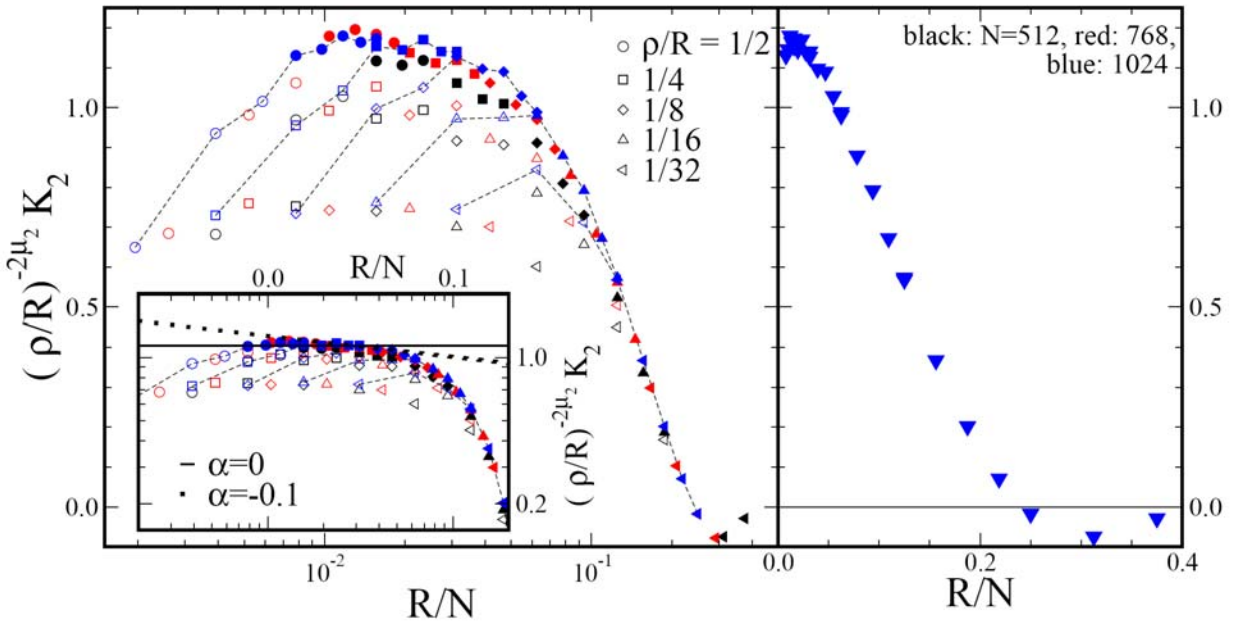


Fig. 5. *Left panel:* Scaling of the product of eight wave functions K_2 normalized to the Hartree-Fock matrix element squared (governed by the exponent $2\mu_2=1.25$) with the distance R between the two couples of spatial points in units of the system size N . Different symbols correspond to different values of the ratio ρ/R (where ρ is the size of the couple); different colors correspond to different system sizes N , as in Fig. 4 (right panel). *Inset:* Same data on a log-log scale. Solid line and dotted line indicate the power-law scaling region and show the uncertainty range for the numerical value of the correction to the exponent $2\mu_2$. *Right panel:* Single-parameter scaling function (as obtained from the data points shown by full symbols in the left panel) on the double-linear scale.

Our numerical results (see Fig. 5) show that the dephasing rate of spinless electrons due to short-range interaction at the quantum-Hall transition is governed by the exponent μ_2 which determines the scaling of the Hartree-Fock matrix element of the interaction (the corrections to $2\mu_2$ vanish within the numerical accuracy). A similar result was obtained analytically within the four-loop renormalization group in $2+\varepsilon$ dimensions. Importantly, the most relevant multifractal exponent drops out from the dephasing rate because of the Hartree-Fock cancellation.

Finally, we have discussed the current understanding of the Coulomb interaction case and confronted it with the available experimental data.

5. Non-equilibrium effects and dephasing in edge state interferometers

Many recent experiments [14-17] studied transport through an electronic analog of Mach-Zehnder interferometer built on edge states in the quantum Hall regime (Fig.6, top left). These experiments show strong Aharonov-Bohm oscillations, which is a manifestation of quantum interference of edge states propagating along the arms of the interferometer. A further remarkable experimental observation is a lobe structure in the dependence of visibility of oscillations on bias voltage (Fig.6, top right). This structure can not be explained within a model of non-interacting electrons and thus results from electron-electron interaction. Therefore, the experiments on Mach-Zehnder interferometers exhibit physics resulting from interplay of quantum interference and Coulomb interaction of topologically protected edge states under strongly non-equilibrium conditions. Development of a theory of such phenomena is a challenging task.

In Ref. [18] we developed a theoretical description of interaction-induced phenomena in an electronic Mach-Zehnder interferometer formed by integer quantum Hall edge states (with $\nu = 1$ and 2 channels) out of equilibrium and confronted theoretical predictions with the experiment. Our theory formulated in terms of functional-bosonization Keldysh action takes into account all effects of the electron-electron interaction, including formation and characteristics of the lobe structure, as well as the non-equilibrium dephasing. The Keldysh action is expressed in terms of a total single-particle time-dependent interferometer scattering matrix $S(t, t', [\phi])$. It describes scattering of electrons at quantum point contacts as well as their propagation along the arms of the interferometer in the fluctuating Hubbard-Stratonovich field ϕ (Fig.6, bottom left). The S-matrix is non-local in time and takes different values ($S_f = S[\phi_f]$ and $S_b = S[\phi_b]$) on the forward (backward) branch of the Keldysh contour. The action has the form

$$i\mathcal{A}(\varphi, \vec{\chi}) = \ln \det \left[1 + (S_b^\dagger e^{i\hat{\chi}} S_f - 1) \hat{f} \right] - i\vec{\varphi}^t \tilde{\Pi} \vec{\varphi} + i\vec{\varphi}^t V_0^{-1} \sigma_x \vec{\varphi}.$$

Here χ is the ‘‘counting field’’(source), Π is polarization operator, and V_0 is the electron-electron interaction. The most non-trivial part of the action is given by the first term that has a form of the Fredholm determinant similar to those that arise in the problem of counting statistics.

We first applied the theory to the model of short-range interaction. In this way we reproduce the lobe structure and also find the suppression of the interference signal due to dephasing (Fig.6, bottom right). While showing some similarity to experimental observations, the results of the short-range-interaction model contradict to the experiment in several crucial aspects. Specifically, in the case of equal arm lengths, which is predominantly the experimental situation, the visibility calculated in the framework of this model oscillates with voltage without any decay, since the non-equilibrium dephasing rate vanishes whatever strong the interaction is. The situation gets even

worse when one tries to apply the same model to describe the MZI at $\nu = 1$, since in this situation the model predicts a constant (voltage-independent) visibility.

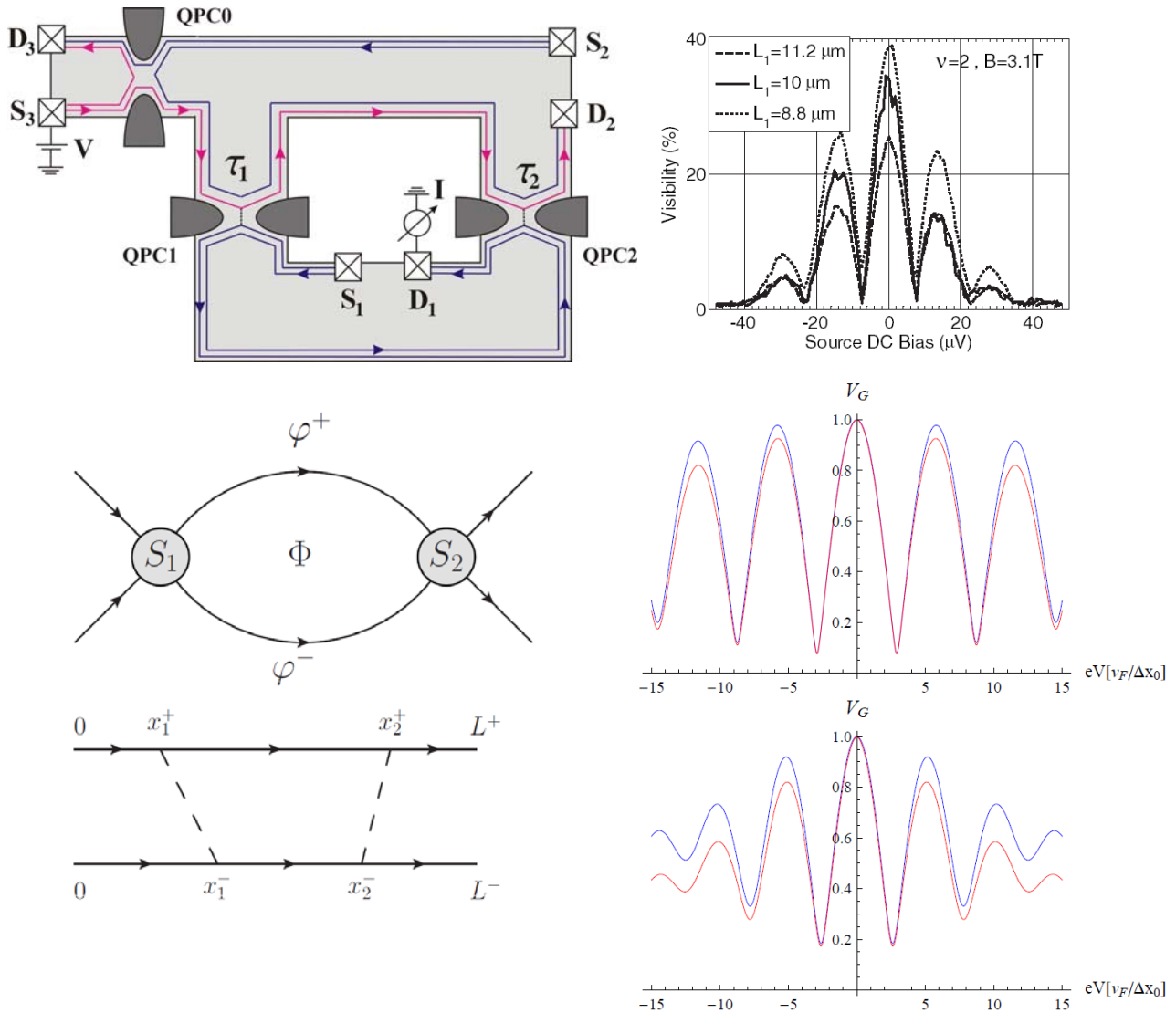


Fig. 6. *Left top:* Scheme of quantum Hall edge-state Mach-Zehnder interferometer at filling factor $\nu = 2$. Quantum point contacts QPC1 and QPC2 partially mix the outer edge channels. All Ohmic contacts are grounded, except for the source terminal S_3 which is kept at voltage V . The current is measured in the drain terminal D_1 . The QPC0 is pinched in such a way that the inner channel is completely reflected while the outer one is fully transmitted. *Left bottom:* scheme of two interfering paths representing edge states in two arms of the interferometer that propagate in Hubbard-Stratonovich fields φ_+ and φ_- , respectively. *Right top:* Experimentally measured visibility in $\nu = 2$ interferometer [14]. *Right bottom:* visibility calculated in the model of strong short-range interaction, with equal quantum point contact (transmission coefficients 0.2) and $\nu = 2$. Blue curve: dephasing is neglected; red curve: dephasing by the shot-noise is taken into account. Upper panel: ratio of two arm lengths $l_+/l_- = 1.15$; lower panel: $l_+/l_- = 1.35$.

This motivated us to explore the more realistic case of $1/r$ Coulomb interaction that leads to a non-linear dispersion of plasmon modes. Using our general formalism, we analyzed the cases of $\nu = 1$ and $\nu = 2$ edge modes, see Fig.7. The obtained parametric dependences of the interference signal are in good agreement with experiments, although in the case of $\nu = 1$ mode some discrepancies remain.

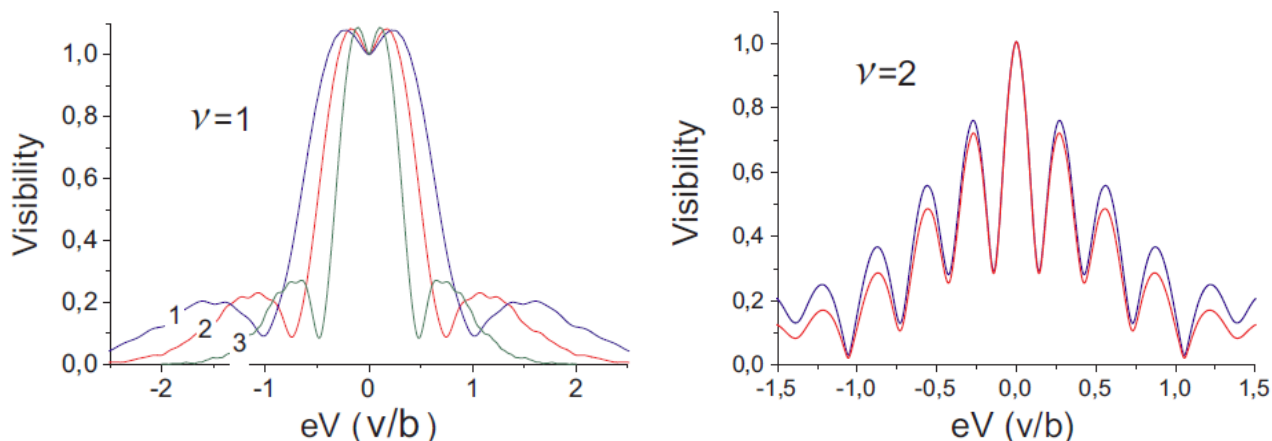


Fig.7. Visibility of Aharonov-Bohm oscillations in a symmetric Mach-Zehnder interferometer calculated in the model of long-range Coulomb interaction with the coupling constant $\alpha = 1$. *Left:* setup with $\nu = 1$ edge channels, shown for $a/b = 0.1$ and different ratios of L/b : (1)-30; (2)-50; (3)-100. Here L is the arm lengths, b the edge state width, and a the short-scale cutoff (of the order of magnetic length). *Right:* $\nu = 2$ edge channels, shown for $L/b = 30$ and $a/b = 0.1$. Upper curve: Gaussian approximation; lower curve: dephasing induced by shot-noise of the quantum point contact (transmission coefficient 0.2) is taken into account.

The formalism developed in this work will be important for future investigation of quantum coherence in interferometers formed by edge states of further topological insulators. This includes, first, fractional quantum Hall effects, and second, edge states of quantum spin Hall effect. Both these planned research directions are of direct experimental relevance.

Cooperations

The work in this project is carried out in cooperation with several CFN projects, including theoretical and experimental activities in the field of quantum computing and superconducting nanostructures (in particular, topologically protected qubits) as well as spintronics:

- B2.2: Shnirman, Schön (theory of spintronics in nanostructures)
- B3.6: Ustinov, von Löhneysen, B3.3: Shnirman, Schön, B3.7: Shnirman (experimental and theoretical studies of topologically protected qubits for quantum computing and quantum information processing)

We also maintain close contacts and cooperation with leading theoretical and experimental groups worldwide: Würzburg University, FU Berlin (Germany), Bar Ilan University, Weizmann Institute (Israel), Ioffe Institute (St. Petersburg, Russia), University of California in Santa Barbara, Princeton

University (USA), Birmingham University (UK), Landau Institute, and Institute for Solid State Physics (Chernogolovka, Russia).

References

- own work with complete titles -

- [1] M. König *et al*, *Science* **318**, 766 (2007).
- [2] D. Hsieh *et al*, *Nature* **452**, 970 (2008); *Nature* **460**, 1101 (2009).
- [3] B. Büttner *et al.*, arXiv:1009.2248 (2010).
- [4] F. Evers and A.D. Mirlin, *Anderson transitions*, *Rev. Mod. Phys.* **80**, 1355 (2008).
- [5] A.Yu. Kitaev, in *Advances in Theoretical Physics*, edited by V. Lebedev and M. Feigelman, AIP Conf. Proc. **1134**, (AIP, New York, 2009), p. 22.
- [6] A.P. Schnyder *et al.*, *Phys. Rev. B* **78**, 195125 (2008); A. P. Schnyder *et al.* in *Advances in Theoretical Physics*, edited by V. Lebedev and M. Feigelman, AIP Conf. Proc. **1134** (AIP, New York, 2009), p. 10; S. Ryu *et al.*, *New J. Phys.* **12**, 065010 (2010).
- [7] P.M.Ostrovsky, I.V. Gornyi, and A.D. Mirlin, *Quantum criticality and minimal conductivity in graphene with long-range disorder*, *Phys. Rev. Lett.* **98**, 256801 (2007).
- [8] J.H. Bardarson, J. Tworzydło, P.W. Brouwer, and C.W.J. Beenakker, *Phys. Rev. Lett.* **99**, 106801 (2007); K. Nomura, M. Koshino, and S. Ryu, *Phys. Rev. Lett.* **99**, 146806 (2007), P. San-Jose, E. Prada, and D.S. Golubev, *Phys. Rev. B* **76**, 195445 (2007).
- [9] B.L. Altshuler and A.G. Aronov, in *Electron-electron interactions in disordered conductors*, edited by A.L. Efros and M. Pollak (Elsevier, 1985), p. 1.
- [10] A. M. Finkelstein, *Sov. Sci. Rev. A. Phys.* **14**, 1 (1990).
- [11] I.S. Burmistrov, S. Bera, F. Evers, I.V. Gornyi, and A.D. Mirlin, *Wave function multifractality and dephasing at metal-insulator and quantum Hall transitions*, preprint arXiv:1011.3616, to be published in *Annals of Physics* (2011).
- [12] D-H. Lee and Z.Wang, *Phys. Rev. Lett.* **76**, 4014 (1996).
- [13] Z.Wang, M.P.A. Fisher, S.M.Girvin, and J.T.Chalker, *Phys. Rev. B* **61**, 8326 (2000).
- [14] Y. Ji, Y. C. Chung, D. Sprinzak, M. Heiblum, D. Mahalu, and H. Shtrikman, *Nature (London)* **422**, 415 (2003); I. Neder, M. Heiblum, Y. Levinson, D. Mahalu, and V.Umansky, *Phys. Rev. Lett.* **96**, 016804 (2006); I. Neder, M. Heiblum, D. Mahalu, and V. Umansky, *Phys. Rev. Lett.* **98**, 036803 (2007); I. Neder, F. Marquardt, M. Heiblum, D. Mahalu, and V. Umansky, *Nat. Phys.* **3**, 534 (2007).
- [15] P. Roulleau, F. Portier, D. C. Glattli, P. Roche, A. Cavanna, G. Faini, U. Gennser, and D. Mailly, *Phys. Rev. B* **76**, 161309(R) (2007); P. Roulleau, F. Portier, D. C. Glattli, P. Roche, A. Cavanna, G. Faini, U. Gennser, and D. Mailly, *Phys. Rev. Lett.* **100**, 126802 (2008); P. Roulleau, F. Portier, P. Roche, A. Cavanna, G. Faini, U. Gennser, and D. Mailly, *Phys. Rev. Lett.* **101**, 186803 (2008); *ibid* **102**, 236802 (2009).
- [16] L. V. Litvin, H.-P. Tranitz, W. Wegscheider, and C. Strunk, *Phys. Rev. B* **75**, 033315 (2007); L. V. Litvin, A. Helzel, H.-P. Tranitz, W. Wegscheider, and C. Strunk, *Phys. Rev. B* **78**, 075303 (2008); *ibid* **81**, 205425 (2010).
- [17] E. Bieri, M. Weiss, O. Göktas, M. Hauser, C. Schönenberger, and S. Oberholzer, *Phys. Rev. B* **79**, 245324 (2009).
- [18] M. Schneider, D.A. Bagrets, and A.D. Mirlin, *Theory of non-equilibrium Mach-Zehnder interferometer*, submitted to *Phys. Rev. B*.